FRONTIERS OF PHYSICS

RESEARCH ARTICLE
Volume 19 / Issue 5 / 52201 / 2024

Spatiotemporal nonlinear dynamics in multimode fiber laser based on carbon nanotubes

Jingxuan Sun[1], Yachen Wang[1], Congyu Zhang[1], Lijun Xu[1], Bo Fu[1,2,†]

1 Key Laboratory of Precision Opto-Mechatronics Technology, School of Instrumentation and Optoelectronic Engineering, Beihang University, Beijing 100191, China
2 Key Laboratory of Big Data-Based Precision Medicine, Ministry of Industry and Information Technology, School of Engineering Medicine, Beihang University, Beijing 100191, China
Corresponding author. E-mail: †fubo10@buaa.edu.cn
Received December 20, 2023; accepted March 5, 2024

ABSTRACT

We investigated 1-μm multimode fiber laser based on carbon nanotubes, where multiple typical pulse states were observed, including Q-switched, Q-switched mode-locked, and spatiotemporal mode-locked pulses. Particularly, stable spatiotemporal mode-locking was realized with a low threshold, where the pulse duration was 37 ps and the wavelength was centred at 1060.5 nm. Moreover, both the high signal to noise and long-term operation stability proved the reliability of the mode-locked laser. Furthermore, the evolution of the spatiotemporal mode-locked pulses in the cavity was also simulated and discussed. This work exhibits the flexible outputs of spatiotemporal phenomena in multimode lasers based on nanomaterials, providing more possibilities for the development of high-dimensional nonlinear dynamics.

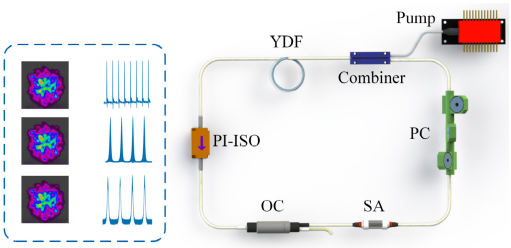

Keywords spatiotemporal mode-locking, multimode fiber, saturable absorber, ultrafast laser

1 Introduction

Spatiotemporal mode-locked ultrafast lasers have attracted extensive attention in recent years, in which both the transverse and longitudinal modes are locked, conducive to the generation of high-energy pulses [1, 2]. Multimode fibers (MMFs) have also gradually become important platforms for spatiotemporal mode-locking owing to the larger mode field area [3]. In 2017, Wright *et al.* [1] first achieved spatiotemporal pulses mode-locked by nonlinear polarization rotation based on graded-index MMFs (GIMFs) with small modal dispersion. Subsequently, step-index MMFs were also proved to be used for generating spatiotemporal mode-locking, where the larger modal dispersion can be counteracted through intracavity spatial filter or saturable absorber (SA) [4, 5]. These results provided more possibilities for the study of spatiotemporal dynamics [6–9]. Moreover, all-fiber lasers are meaningful for the applications of spatiotemporal mode-locking in various fields due to the advantages of high environmental stability, compact design, alignment-free operation, and high beam quality [10–12]. In order to realize the all-fiber structure, the select of suitable saturable absorber is of great significance. At present, nonlinear polarization rotation, nonlinear amplifying loop mirror, nonlinear multimode interference, and Mamyshev regenerators have been applied to achieve ultrafast pulses in all-fiber MMF lasers [13–16]. Furthermore, nanomaterials are also promising candidates for intracavity saturable absorption devices, which possess broadband operation, tunable modulation depth, as well as easy fabrication and inte-

Higher Education Press

https://doi.org/10.1007/s11467-024-1399-2

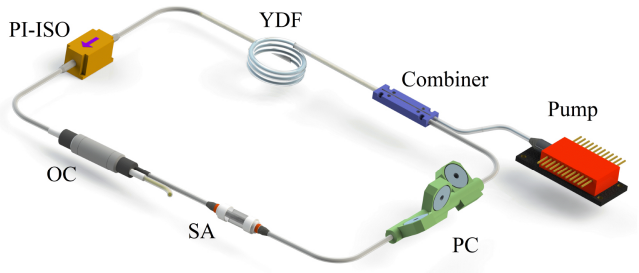

Fig. 1 Setup of the spatiotemporal mode-locked laser at 1 μm. YDF: Ytterbium-doped fiber; PI-ISO: Polarization-insensitive isolator; OC: Output coupler; SA: Saturable absorber; PC: Polarization controller.

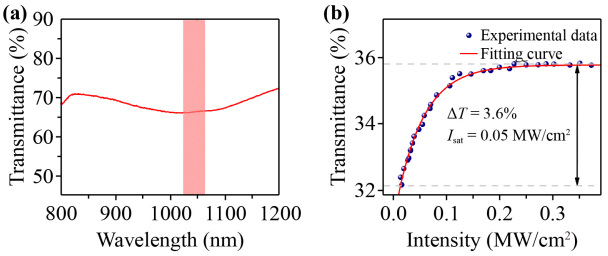

Fig. 2 Optical properties of carbon nanotubes. **(a)** Linear transmittance curve of CNTs. **(b)** Nonlinear transmittance curve of CNTs at 1 μm. α_s: Modulation depth; $I_{\rm sat}$: Saturable intensity.

gration [17–22]. The excellent performance of nanomaterials provides more freedom in studying spatiotemporal mode-locking dynamics.

Herein, we constructed an all-fiber Yb-doped fiber laser (YDFL) based on carbon nanotubes (CNTs)-SA to investigate multiple spatiotemporal phenomena. The spatiotemporal Q-switching, Q-switched mode-locking, and mode-locking were all observed by adjusting the polarization state and pump power carefully, which benefited from various effects in the MMF laser. In order to analyze the spatiotemporal mode-locking in detail, the propagation of pulses in this cavity was also simulated, where the evolution of pulses versus roundtrips and different positions were discussed.

2 Experimental section

The setup of the all-fiber multimode ring laser is shown in Fig. 1. The gain medium is 1.8-m YDF (Liekki YB1200-10/125DC), which is pumped by a 980-nm laser through a combiner. The ring cavity also includes a polarization insensitive isolator for ensuring unidirectional light propagation, a polarization controller for adjusting polarization state, a SA device for generating ultrafast pulses, and an 80/20 coupler for output pulses. Apart from the customized combiner, all the tail fibers of the passive components are GIMFs (50/125 μm), which have parabolic refractive index distributions and relatively small modal dispersion compared to step-index MMFs. Based on the setup of the laser, the excitation of high-order transverse modes or the spatial filtering will occur at the splice of fibers with different core diameters. In addition, the structure of GIMFs-YDF-GIMFs will also introduce a multimode interference filter, which has influence on the spectrum characteristics of pulses [23–25]. Therefore, diverse spatiotemporal phenomena were further observed and analyzed under the combination of multiple effects.

In this experiment, the SA device based on nanomaterials was integrated by sandwich structure, where CNTs were sandwiched between two fiber ferrules and then assembled by a fiber adapter. Figure 2(a) shows the linear transmittance of CNTs, which was tested by ultraviolet-visible-near-infrared spectrophotometer (UV-3600). Figure 2(b) illustrates the nonlinear transmittance of CNTs in 1-μm band, which was measured with a 1-μm mode-locked laser as light source. The repetition rate and pulse width of the mode-locked laser source are 40 MHz and 9.4 ps at the central wavelength of 1060 nm. The mode-locked laser connected with a 50/50 optical coupler through a variable optical attenuator, where the power coupled into SA was controlled by adjusting the attenuator. One port of the output was directly monitored as the reference side, while another port was monitored as the test side after passing through SA. The nonlinear transmittance was the ratio of the test and reference sides. The trend of transmittance as a function of the input light intensity is fitted by the formula $T = 1 - \alpha_s/(1 + I/I_{\rm sat}) - \alpha_{ns}$ [26], where T is transmittance, α_s is saturable absorption (i.e., modulation depth), I is incident light intensity, I_{sat} is saturable intensity, and α_{ns} is non-saturable absorption. As shown in Fig. 2(b), the modulation depth and saturable intensity of CNTs-based SA are ~3.6% and 0.05 MW/cm^2, respectively, exhibiting promising abilities for generating pulses.

3 Results and discussion

The continuous wave appeared when the pump power was gradually increased to 720 mW with an appropriate adjustment of PC. Then the Q-switched pulses centered at 1037.6 nm was realized firstly at the pump power of 730 mW. The spectrum and the multimode irregular beam profile are shown in Fig. 3(a). Figure 3(b) is the temporal waveform of the Q-switched pulses, where the pulse interval is 77.3 μs. The duration of the single pulse profile is 9.4 μs as shown in Fig. 3(c). The 12.9-kHz radio frequency (RF) spectrum with a 26-dB signal-to-noise ratio (SNR) is also shown in Fig. 3(d). In addition, the output power of the pulses was 1.6 mW, corresponding to 127.2-nJ pulse energy.

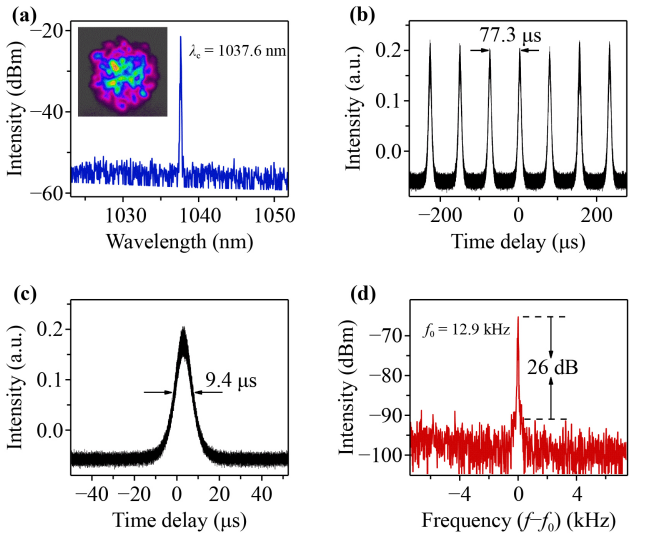

Fig. 3 Q-switched results. **(a)** Spectrum. Inset: Beam profile. **(b)** Temporal waveform. **(c)** Pulse profile. **(d)** RF spectrum.

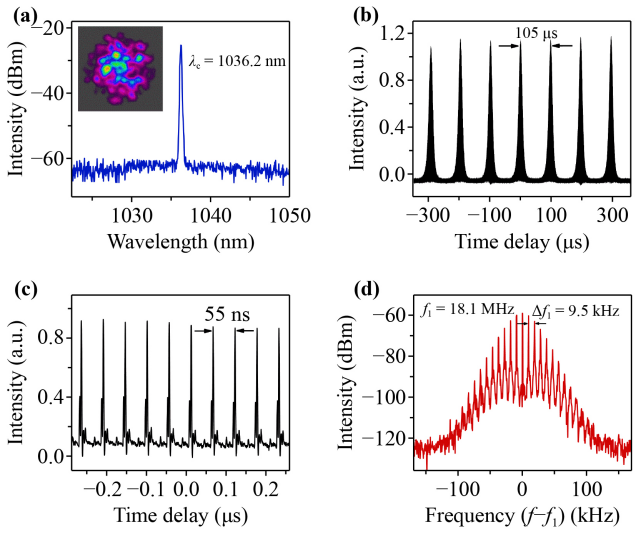

Fig. 4 Q-switched mode-locked results. **(a)** Spectrum (Inset: Beam profile). **(b)** Temporal waveform. **(c)** Zoomed view of the temporal waveform. **(d)** RF spectrum.

The Q-switched mode-locking was also obtained by tuning the PC. Figure 4(a) shows the spectrum centered at 1036.2 nm, and the inset is the beam profile with multi-transverse modes. The envelope of the Q-switched pulses in time domain is exhibited in Fig. 4(b), where the pulse interval is 105 μs. The detailed mode-locked pulses with 55-ns spacing can be seen from Fig. 4(c) when the span of Q-switched envelope was stretched. Figure 4(d) is the RF spectrum with multiple peaks, in which the central frequency peak is 18.1 MHz and the interval of different peaks is 9.5 kHz, corresponding to the pulse intervals of mode-locked and Q-switched trains, respectively. The Q-switched mode-locking is a typical state in laser, while the stable mode-locking will be realized when the polarization state is tuned or the pulse energy in the cavity increases [27, 28].

Therefore, the mode-locked operation was obtained when the pump power was further increased to 750 mW and PC was further adjusted in an appropriate orientation. It is also found that the threshold of the mode-locking in this laser is relatively low compared with previous results in other MMF lasers. Figure 5 presents the typical 1-μm spatiotemporal mode-locked results based on CNTs-SA. Figure 5(a) shows the spectrum centered at 1060.5 nm and beam profile with speckle pattern of the mode-locked pulses. The narrow spectrum is mainly caused by the multimode interference effect [23]. The irregular beam profile indicates the multiple

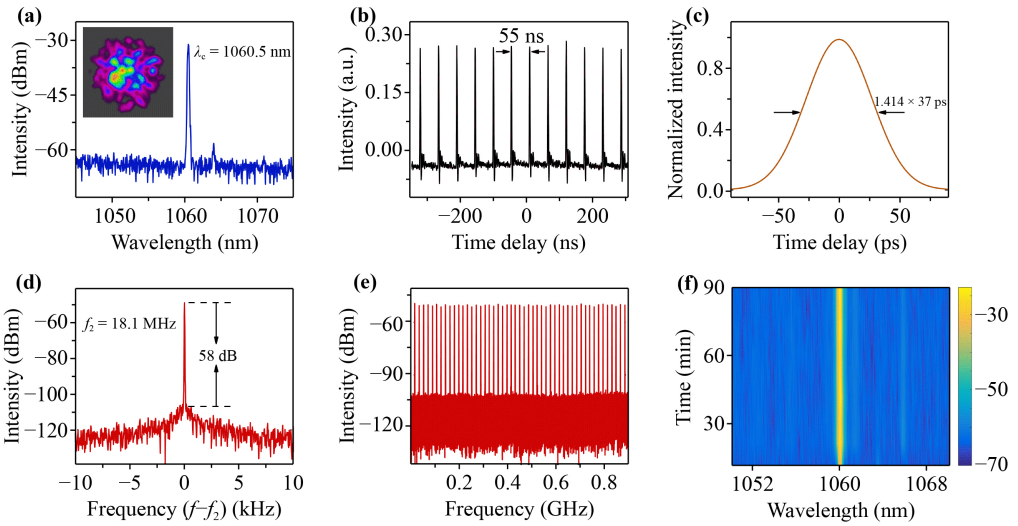

Fig. 5 Spatiotemporal mode-locked results. **(a)** Spectrum (Inset: Beam profile). **(b)** Temporal waveform. **(c)** Pulse profile. **(d)** RF spectrum. **(e)** RF spectrum under a larger span. **(f)** Spectra evolution versus time.

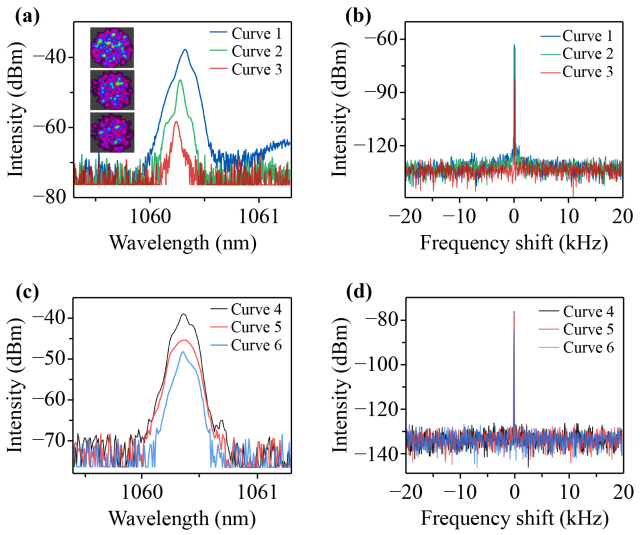

Fig. 6 Results of spectral filtering and spatial sampling. **(a)** Optical (Inset: Beam profiles) and **(b)** RF spectra of spectral filtering. **(c)** Optical and **(d)** RF spectra of spatial sampling.

transverse modes of the pulses. In addition, the 55-ns pulse interval in Fig. 5(b) demonstrates the 18.1-MHz repetition rate, which is in accord with the mode-locked frequency in QSML, corresponding to 11-m cavity length. The 37-ps pulse duration and the autocorrelation trace of the pulses are shown in Fig. 5(c). Figure 5(d) exhibits the RF spectrum with a 58-dB signal to noise. The RF spectrum has no significant fluctuation when the span of frequency domain is expanded, as shown in Fig. 5(e), proving the stability of the pulses. Moreover, the spectra evolution versus time was also recorded in Fig. 5(f) when the laser worked continuously, where the well-maintained intensity and center wavelength indicate the long-term stability of the laser.

In addition, the spatiotemporal characteristics were also verified by the methods of spectral filtering and spatial sampling, in which the setup and operation are similar to that described in Ref. [29]. Figure 6(a) shows the optical spectra of pulses obtained by spectral filtering, where the inserted different beam profiles prove the difference of transverse-mode components. The corresponding RF spectra in Fig. 6(b) overlap, indicating the locking of transverse modes. The optical and RF spectra of pulses obtained by spatial sampling are shown in Figs. 6(c) and (d), which were sampled at different positions of beam profile. The optical spectra under different transverse-mode components are different, while the consistent RF spectra further demonstrates the realization of spatiotemporal mode-locking.

In order to further analyze the spatiotemporal mode-locking obtained in 1-μm laser, the propagation of the light in the cavity was modeled according to the experimental setup of the MMF laser. The components with different transmission characteristics were described by different functions, then the light propagated circularly in the cavity, where the evolution of the light field can be simulated and analyzed. The light field in the GIMFs was simulated by the generalized multimode nonlinear Schrödinger equation [30, 31]. Given the computation time, six low-order modes were considered into the propagation in the cavity and the initial signal was defined as a Gaussian pulse. For the gain fiber, the bandwidth of gain is 40 nm, $g_0 = 4\ \mathrm{m}^{-1}$, and $E_{sat} = 0.12$ nJ. When light is transmitted at the splice of fibers with different core diameters, it will be affected by spatial coupling and filtering effects. The effect caused by the spatial filter can be described as $A_{out}(z,t) = \boldsymbol{M}A_{in}(z,t)$, in which $\boldsymbol{M}$ is the coupling coefficient matrix between different modes. The transmission state of the pulses in the cavity will change obviously while changing the spatial filter, indicating the important role of spatial filter in the process of spatiotemporal mode-locking.

Figure 7 exhibits the simulated results of the stable spatiotemporal mode-locking in a multimode all-fiber laser. The signal light gradually evolved into stable mode-locked pulses with the increase of the roundtrips, where different modes are represented by different colors as shown in Fig. 7(a). During the formation of stable pulses, the modal walk-off caused by dispersion is usually compensated by spatial filtering besides Kerr effect. Specifically, spatial filtering affects the coupling effect between modes, where the walk-off can be compensated under proper coupling matrix, and thus different modes are coupled together for transmission. Moreover, saturable absorber also plays an important role in compensating dispersion, which performs saturation absorption on three-dimensional pulses, bringing different absorption and energy distribution to different modes. In the simulation, the compensation process of modal walk-off is also demonstrated from the view of the time-domain peak position with different modes, as shown in the upper in Fig. 7(b). The transmission of pulses with different modes is irregular and the speeds are different before the 53$^{\mathrm{rd}}$ roundtrip. The peak positions of pulses corresponding to different modes have the same displacement velocity after the 53$^{\mathrm{rd}}$ roundtrip, which is shown as the same slopes, indicating the same group velocity of different modes, namely, the locking of transverse mode. Therefore, it also indicates that the modal walk-off is compensated under the action of intracavity effects and the stable pulse is formed. Accordingly, the energy of different modes also stabilizes, in keeping with the evolution process of pulse in time domain, as shown in the below of Fig. 7(b). Figure 7(c) is the evolution of pulses with different positions in the 300th roundtrip, which exhibits the effects of different components on the transmission of pulses. The spectrum of stable spatiotemporal mode-locked pulse is shown in Fig. 7(d). Figure 7(e) shows pulse profile of the spatiotemporal

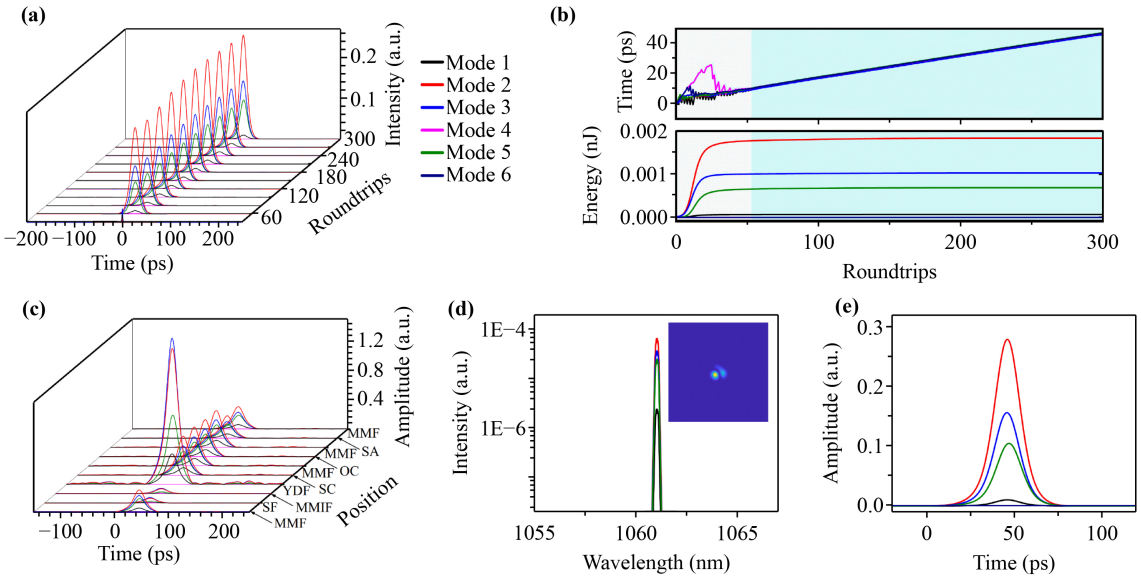

Fig. 7 Simulated results of the spatiotemporal mode-locking. **(a)** Evolution of pulses in time domain with different roundtrips. **(b)** Evolution of the time-domain peak positions and the energy of pulses corresponding to different modes. **(c)** Evolution of stable pulses with different positions in the 300th roundtrip. MMF: Multimode fiber; SF: Spatial filter; SC: Spatial coupling; MMIF: Multimode interference filter; YDF: Yb-doped fiber; OC: Output coupler; SA: Saturable absorber. **(d)** Spectrum (Inset: Beam profile). **(e)** Pulse profile.

mode-locked pulse. During the simulation, the generation of spatiotemporal mode-locked pulses is confirmed from the energy and time domain of different modes, where the processes of locking of modes and evolution of pulses are also more clearly.

In this experiment, the saturable absorption effect of CNTs was utilized to generate pulses in laser cavity. As a kind of SA, CNTs have advantages of simple structure, high environmental stability, ultrafast recovery time, and broadband operation, which are conducive to realizing high-performance mode-locking in all-fiber lasers [32–34]. It can also be found that the laser based on CNTs-SA had a lower mode-locked threshold, where the 1-μm spatiotemporal pulses were obtained at a low pump power. Furthermore, the conversion between various typical pulse states was also observed, providing more directions for the study of nonlinear dynamics in multimode lasers.

4 Conclusions

In summary, we demonstrated a spatiotemporal fiber laser at the wavelength of 1 μm based on CNTs as SA. Based on the combined action of various effects such as spatial filtering and saturable absorption, the spatiotemporal Q-switching, Q-switched mode-locking, and mode-locking were realized at a low threshold. The characteristics of the obtained pulses in the experiment were monitored and discussed, including pulse width, beam profile, frequency, and stability. Furthermore, to give insight into the propagation of spatiotemporal mode-locked pulses in MMF laser, the numerical simulation was also performed and detailed process on the evolution of spatiotemporal pulses was exhibited. Such kind of laser provides a platform for the combination of nanomaterials and MMF lasers, which are beneficial for the further investigation on spatiotemporal dynamics.

Declarations The authors declare that they have no competing interests and there are no conflicts.

Acknowledgements This work was supported by the National Natural Science Foundation of China (Grant No. 62071016), the State Key Laboratory of Advanced Optical Communication Systems Networks, China, and the Academic Excellence Foundation of BUAA for PhD Students.

References

1. L. G. Wright, D. N. Christodoulides, and F. W. Wise, Spatiotemporal mode-locking in multimode fiber lasers, *Science* 358(6359), 94 (2017)
2. L. G. Wright, P. Sidorenko, H. Pourbeyram, Z. M. Ziegler, A. Isichenko, B. A. Malomed, C. R. Menyuk, D. N. Christodoulides, and F. W. Wise, Mechanisms of spatiotemporal mode-locking, *Nat. Phys.* 16(5), 565 (2020)
3. K. Krupa, A. Tonello, A. Barthélémy, T. Mansuryan, V. Couderc, G. Millot, P. Grelu, D. Modotto, S. A. Babin, and S. Wabnitz, Multimode nonlinear fiber optics, a spatiotemporal avenue, *APL Photonics* 4(11), 110901

(2019)
4. Y. Ding, X. Xiao, K. Liu, S. Fan, X. Zhang, and C. Yang, Spatiotemporal mode-locking in lasers with large modal dispersion, *Phys. Rev. Lett.* 126(9), 093901 (2021)
5. C. Gao, B. Cao, Y. Ding, X. Xiao, D. Yang, H. Fei, C. Yang, and C. Bao, All-step-index-fiber spatiotemporally mode-locked laser, *Optica* 10(3), 356 (2023)
6. U. Teğin, E. Kakkava, B. Rahmani, D. Psaltis, and C. Moser, Spatiotemporal self-similar fiber laser, *Optica* 6(11), 1412 (2019)
7. J. Long, Y. Gao, W. Lin, J. Wu, X. Lin, W. Hong, H. Cui, Z. Luo, W. Xu, and A. Luo, Switchable and spacing tunable dual-wavelength spatiotemporal mode-locked fiber laser, *Opt. Lett.* 46(3), 588 (2021)
8. W. Fang, X. Ma, Y. Zhou, W. Zhang, X. Chen, S. Huang, M. Liao, Y. Ohishiand, and W. Gao, Transverse mode switchable fiber laser with a multimodal interference-based beam shaper, *Opt. Lett.* 48(1), 53 (2023)
9. B. Fu, C. Shang, H. Liu, S. Fan, K. Zhao, Y. Zhang, S. Wageh, A. Al-Ghamdi, X. Wang, L. Xu, X. Xiao, and H. Zhang, Recent advances and future outlook in mode-locked lasers with multimode fibers, *Appl. Phys. Rev.* 10(4), 041305 (2023)
10. M. E. Fermann and I. Hartl, Ultrafast fibre lasers, *Nat. Photonics* 7(11), 868 (2013)
11. U. Teğin and B. Ortaç, All-fiber all-normal-dispersion femtosecond laser with a nonlinear multimodal interference-based saturable absorber, *Opt. Lett.* 43(7), 1611 (2018)
12. U. Teğin, B. Rahmani, E. Kakkava, D. Psaltis, and C. Moser, All-fiber spatiotemporally mode-locked laser with multimode fiber-based filtering, *Opt. Express* 28(16), 23433 (2020)
13. S. Xie, L. Jin, H. Zhang, X. Li, X. Zhang, Y. Xu, and X. Ma, All-fiber high-power spatiotemporal mode-locked laser based on multimode interference filtering, *Opt. Express* 30(2), 2909 (2022)
14. X. Lin, Y. Gao, J. Long, J. Wu, W. Hong, H. Cui, Z. Luo, W. Xu, and A. Luo, All few-mode fiber spatiotemporal mode-locked figure-eight laser, *J. Lightwave Technol.* 39(17), 5611 (2021)
15. J. Wu, G. Liu, Y. Gao, X. Lin, H. Cui, Z. Luo, W. Xu, M. E. Likhachev, S. S. Aleshkina, V. M. Mashinsky, M. V. Yashkov, and A. P. Luo, Switchable femtosecond and picosecond spatiotemporal mode-locked fiber laser based on NALM and multimode interference filtering effects, *Opt. Laser Technol.* 155, 108414 (2022)
16. B. Cao, C. Gao, Y. Ding, X. Xiao, C. Yang, and C. Bao, Self-starting spatiotemporal mode-locking using Mamyshev regenerators, *Opt. Lett.* 47(17), 4584 (2022)
17. L. Huang, Y. Zhang, and X. Liu, Dynamics of carbon nanotube-based mode-locking fiber lasers, *Nanophotonics* 9(9), 2731 (2020)
18. B. Fu, Y. Hua, X. Xiao, H. Zhu, Z. Sun, and C. Yang, Broadband graphene saturable absorber for pulsed fiber lasers at 1, 1.5, and 2 μm, *IEEE J. Sel. Top. Quantum Electron.* 20(5), 411 (2014)
19. Y. Li, B. Gao, Y. Han, B. Chen, and J. Huo, Optoelectronic characteristics and application of black phosphorus and its analogs, *Front. Phys.* 16(4), 43301 (2021)
20. B. Fu, J. Sun, C. Wang, C. Shang, L. Xu, J. Li, and H. Zhang, MXenes: Synthesis, optical properties, and applications in ultrafast photonics, *Small* 17(11), 2006054 (2021)
21. X. Zhao, H. Jin, J. Liu, J. Chao, T. Liu, H. Zhang, G. Wang, W. Lyu, S. Wageh, O. A. Al-Hartomy, A. G. Al-Sehemi, B. Fu, and H. Zhang, Integration and applications of nanomaterials for ultra-fast photonics, *Laser Photonics Rev.* 16(11), 2200386 (2022)
22. X. Li, Y. Guo, Y. Ren, J. Peng, J. Liu, C. Wang, and H. Zhang, Narrow-bandgap materials for optoelectronics applications, *Front. Phys.* 17(1), 13304 (2022)
23. T. Zhao, G. Liu, L. Dai, B. Zhao, H. Cui, C. Mou, Z. Luo, W. Xu, and A. Luo, Narrow bandwidth spatiotemporal mode-locked Yb-doped fiber laser, *Opt. Lett.* 47(15), 3848 (2022)
24. W. S. Mohammed, P. W. Smith, and X. Gu, All-fiber multimode interference bandpass filter, *Opt. Lett.* 31(17), 2547 (2006)
25. A. Mafi, P. Hofmann, C. J. Salvin, and A. Schülzgen, Low-loss coupling between two single-mode optical fibers with different mode-field diameters using a graded-index multimode optical fiber, *Opt. Lett.* 36(18), 3596 (2011)
26. E. Garmire, Resonant optical nonlinearities in semiconductors, *IEEE J. Sel. Top. Quantum Electron.* 6(6), 1094 (2000)
27. J. Lee, J. Koo, P. Debnath, Y. Song, and J. Lee, A Q-switched, mode-locked fiber laser using a graphene oxide-based polarization sensitive saturable absorber, *Laser Phys. Lett.* 10(3), 035103 (2013)
28. K. H. Lin, J. J. Kang, H. H. Wu, C. K. Lee, and G. R. Lin, Manipulation of operation states by polarization control in an erbium-doped fiber laser with a hybrid saturable absorber, *Opt. Express* 17(6), 4806 (2009)
29. J. Sun, G. Wang, J. Chao, X. Wang, H. Yang, and B. Fu, Buildup of multiple spatiotemporal nonlinear dynamics in an all-fiber multimode laser, *Opt. Lett.* 48(22), 6019 (2023)
30. F. Poletti and P. Horak, Description of ultrashort pulse propagation in multimode optical fibers, *J. Opt. Soc. Am. B* 25(10), 1645 (2008)
31. L. G. Wright, W. H. Renninger, D. N. Christodoulides, and F. W. Wise, Spatiotemporal dynamics of multimode optical solitons, *Opt. Express* 23(3), 3492 (2015)
32. H. Kataura, Y. Kumazawa, Y. Maniwa, I. Umezu, S. Suzuki, Y. Ohtsuka, and Y. Achiba, Optical properties of single-wall carbon nanotubes, *Synth. Met.* 103(1-3), 2555 (1999)
33. H. Yang, B. Fu, D. Li, Y. Tian, Y. Chen, M. Mattila, Z. Yong, R. Li, A. Hassanien, C. Yang, I. Tittonen, Z. Ren, J. Bai, Q. Li, E. I. Kauppinen, H. Lipsanen, and Z. Sun, Broadband laser polarization control with aligned carbon nanotubes, *Nanoscale* 7(25), 11199 (2015)
34. A. Martinez and Z. Sun, Nanotube and graphene saturable absorbers for fibre lasers, *Nat. Photonics* 7(11), 842 (2013)